BATCH: jp8d204 USER: rll29 DIV: @xyv04/data1/CLS_pj/GRP_jy/JOB_i33/DIV_jp072564w DATE: July 9, 2007

Long-Range Refractive Index Sensing Using Plasmonic Nanostructures

Tomas Rindzevicius, Yury Alaverdyan, and Mikael Käll*

Department of Applied Physics, Chalmers University of Technology, SE-412 96 Göteborg, Sweden

W. Andrew Murray and William L. Barnes

School of Physics, University of Exeter, Exeter, EX4 4QL United Kingdom

Received: April 2, 2007; In Final Form: June 4, 2007

We study the variation in localized surface plasmon resonance (LSPR) spectra ($\lambda_{LSPR} \approx 600$ nm) as a function of dielectric coating thickness. Langmuir−Blodgett multilayers composed of 22-tricosenoic acid ($n \approx 1.53$) were deposited onto short-range-ordered Au nanodisks and nanoholes on glass in air. For large dielectric coating thicknesses ($d = 100-340$ nm), the LSPRs exhibit a pronounced oscillatory behavior with a periodicity of ~190 nm. This is in agreement with a simple image-dipole model, which yields a periodicity of $\sim\lambda_{LSPR}/2n$. However, the amplitude of the dipolar plasmon resonance wavelength oscillation $\lambda_{LSPR}(d)$ is surprisingly large, of the order 25−45 nm for $d \approx 300$ nm, indicating the importance of finite size effects. The large LSPR shifts observed at such a large distance from the actual metal surface suggest the possibility of using comparatively thick dielectric films as spacer layers in bio/chemo LSPR sensor applications.

1. Introduction

It is well-known that excitation of localized surface plasmon resonances (LSPRs) in noble metal particles or nanostructures result in intense extinction bands that are absent in the bulk or for flat surfaces.[1] The LSPR wavelength, intensity, and linewidth depends on the size, shape, and dielectric properties of the nanostructure, as well as on its dielectric environment and the presence of nearby nanostructures.[1−3] This dependence allows for fine-tuning of various nanoparticle architectures for use as functional materials in numerous applications, including, but not limited to, surface enhanced spectroscopies,[4−7] cancer therapy,[8] and chemo/bio sensors.[9−16] The latter application is of special interest, because it may allow for label-free detection of extremely small concentrations of target molecules. Recent nanoparticle-based sensing mechanisms include nanoparticle aggregation,[9,15,17,18] surface enhanced Raman scattering,[16] and refractive index variation detection.[11−14] The latter sensing principle, which relies on adsorbate induced changes in the local refractive index at the noble metal surface, is the most easily realized in practice. The strong confinement of the electromagnetic fields allows one to miniaturize the LSPR-based refractive index sensors down to the single particle level,[12] where spectral shifts corresponding to zeptomol concentration changes can be detected. The absolute sensitivity to bulk refractive index (RI) changes differs to a great extent between different particle classes (e.g., between spherical particles, nanodisks, nanorods, and nanoshells), but much of this variation seems to be due to a linear scaling between sensitivity and LSPR wavelength.[19] In the case of dielectric-coated metallic particles, it is usually assumed that the LSPR shift exhibits an essentially exponential decay until saturation sets in for dielectric layer thicknesses comparable to the particle size.[14,20] The magnitude of the LSPR shift is then determined by the thickness of the dielectric layer, d, the contrast between the refractive indices of the layer and the bulk environment,[20] and the decay length of the E-field induced through LSPR excitation. This short-distance dependence of the LSPR has been experimentally quantified for single nanoparticles,[12] weakly interacting triangular silver particles prepared by nanosphere lithography (NSL),[13,14] and nanoholes in optically thin gold films.[21] Using self-assembled monolayers (SAMs), the LSPR shift of the Ag nanoparticles was found to saturate at $d \approx 40$ nm. These kinds of experiments are clearly important in order to tune the sensing capabilities of nanoparticles to match the dimensions of biological analytes.

However, it is well-known that the LSPR spectrum not only depends on the dielectric environment in the immediate vicinity of the metal surface. If the surrounding medium is such that the LSPR induced far-field is coherently fed back to the plasmonic nanostructure, a substantial LSPR shift and line-shape change can occur even at large distances. Such diffractive far-field coupling has been observed for ordered arrays and lines of nanoparticles[22,23] and for particles placed above a reflecting metal surface.[24] In a recent paper, Murray et al. showed that the latter effect can also be observed if Ag nanoparticles fabricated by NSL are placed near an interface between two dielectric media.[25] It was observed that a substantial LSPR shift (amplitude ~ 20 nm) remained at distances up to $d \approx 300$ nm from the metal surface. This effect is analogous to the lifetime oscillations observed for fluorescent molecules near an interface between two media,[26] which can be interpreted in terms of so-called cavity quantum electrodynamics. The observation by Murray et al. clearly motivates further investigations of the long-range distance dependence of the LSPR in metal nanostructures. In this paper, we study such effects in short range ordered Au nanodisks and nanoholes prepared by colloidal lithography. Both types of structures are highly interesting for bio/chemo sensing applications.[21,27−29] We show that the LSPR position and line-shape are dramatically affected when the nanostructures are coated with thick (100−340 nm) dielectric layers. The experimental results are discussed in terms of the classical image-dipole model, which is in good qualitative agreement with data.

* To whom correspondence should be addressed. E-mail: kall@fy.chalmers.se.

10.1021/jp072564w CCC: $37.00
Published on Web 00/00/0000 PAGE EST: 4.9

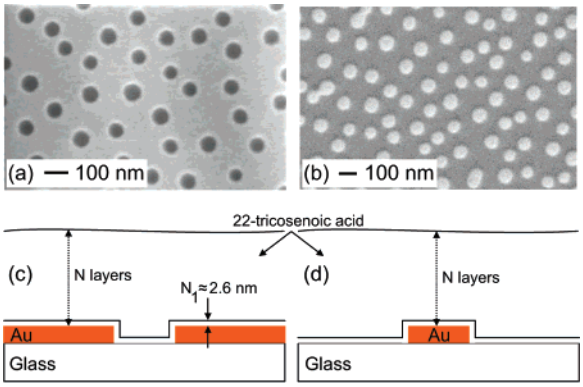

Figure 1. Representative SEM images of ~60 nm short range ordered arrays of nanoholes (density ~40 μm^{-2}) in a 20 nm Au film on glass (a) and ~70 nm Au nanodisks (density ~50 μm^{-2}) on glass (b) together with schematics of the nanostructures coated with N layers of 22-tricosenoic acid (c).

Further, the rapid change in the LSPR spectrum for large layer thicknesses indicates that it is possible to detect target molecules situated hundreds of nanometers away from the metal particle surface. This observation can be of high practical importance for the development of novel nanoplasmonic chemo/bio sensors.

2. Experimental Section

The short range ordered arrays of nanometric holes and disks on glass substrates were fabricated using colloidal lithography,[27] which is capable of producing large areas (>cm ^{2}) of nanostructures. In the case of nanoholes, colloidal polystyrene spheres (sulfate latex, IDC U.S.A.) were adsorbed on a glass substrate, and a 20 nm gold film was evaporated on the surface. The Au covered colloidal polystyrene spheres were then removed by tape stripping. The result is a 20 nm thick Au film containing circular apertures with glass at the bottom; see illustrative SEM image in Figure 1a. In preparing nanometer Au disks, the colloidal polystyrene spheres were instead adsorbed after the 20 nm gold film has been deposited.[30] A heat treatment is then applied to flatten out the polystyrene spheres. The gold metal that is not covered by polystyrene is removed using argon ion beam etching. Finally, the polystyrene particles are removed by tape stripping. This results in 20 nm high circular Au disks, see Figure 1b. The nanohole and nanodisk diameters are controlled by the polystyrene sphere size, and the distances between the objects are tuned by choosing different sphere densities. Due to the heat treatment used for fabricating Au nanodisks, the disk diameters were larger than the diameters of the nanoholes, i.e., ~70 nm versus ~60 nm. The nanohole and nanodisk densities were ~40 and ~50 μm^{-2}, respectively. This choice of parameters results in very similar LSPR wavelengths, i.e., $\lambda_{LSPR} \approx 600$ nm, for the disks and the holes. However, it is not possible to also obtain the same line-width for the two types of samples due to intrinsic differences in LSPR decay processes. Specifically, the line-width of the nanodisk resonance is determined by a combination of radiation damping and internal dissipation,[30] while the hole resonance is also affected by coupling to extended surface plasmon polariton modes of the thin film.[28,31]

The Langmuir−Blodgett (LB) technique was used to sequentially deposit multilayer stacks of 22-tricosenoic acid on the plasmonic nanostructures.[32] A layer of 22-tricosenoic acid from a chloroform solution was first spread on a water surface. The layer was then slowly compressed to a surface pressure of about 30 mNm^{-1}, which results in monolayer formation. The nanohole

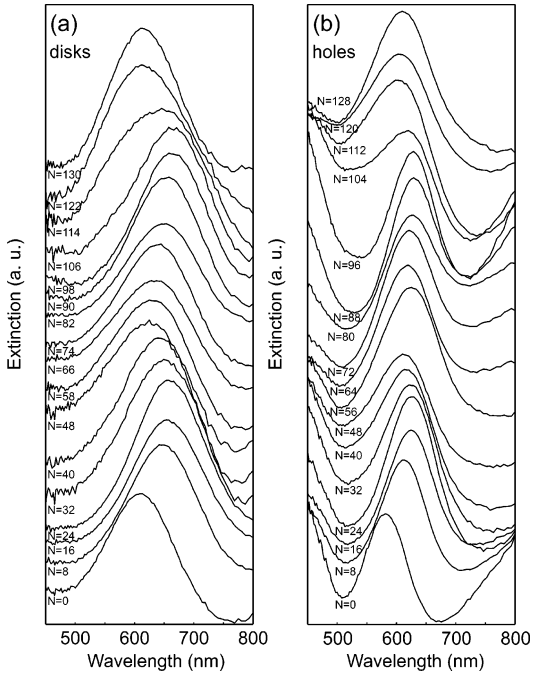

Figure 2. Extinction spectra of gold nanodisks (a) and nanoholes (b) as the number of dielectric layers is sequentially increased from N = 0 to 130 (d = 0 to ~350 nm). The thickness of one 22-tricosenoic acid layer is approximately 2.6 nm.

or nanodisk samples were positioned normal to the water surface and then dipped vertically downward and upward at a rate of 0.25 mm/s while the surface pressure was adjusted to remain constant throughout the whole sample dipping procedure. The number of deposited layers varied from 0 to 140. The latter corresponds to a thickness of ~364 nm. LB films deposited in this way on nanohole films have been studied before.[33] In that study, it was found that the LB film tends to bridge the nanoholes. Further, in that study, which looked at fluorescence from LB film over-coated nanohole films, the assumption of a planar, homogeneous LB film was found to fit the data well; we have therefore assumed the LB film deposits on our samples in the same way.

In the case of the nanohole structures, the sample contained 36 regions that contained a different number of layers and one uncoated reference region. The reproducibility was checked by coating three identical samples with 0−6 layers and then comparing the results. No significant differences were found. In the case of the short range ordered Au nanodisk structures, nine identical samples were used. Each sample contained 5 regions with increasing overlayer coating thickness, and one uncoated reference region to allow for determination of the relative LSPR shift.

The optical properties of the hole and disk samples were quantified using normal incidence extinction spectroscopy. A collimated beam with a divergence of ~0.5° and a diameter of ~1 mm from a tungsten halogen lamp was directed onto the nanostructures. The transmitted intensity was measured vs wavelength using a phase-sensitive lock-in technique,. For a more detailed description, see ref 25. The beam diameter corresponds to averaging over ~1.4×10^4 scattering objects.

3. Results and Discussion

3.1. Experimental Results. Extinction spectra for the Au nanodisk samples as a function of the sequentially increasing number of dielectric layers N are presented in Figure 2a. As expected, the LSPR spectra first exhibit a rapid red-shift with

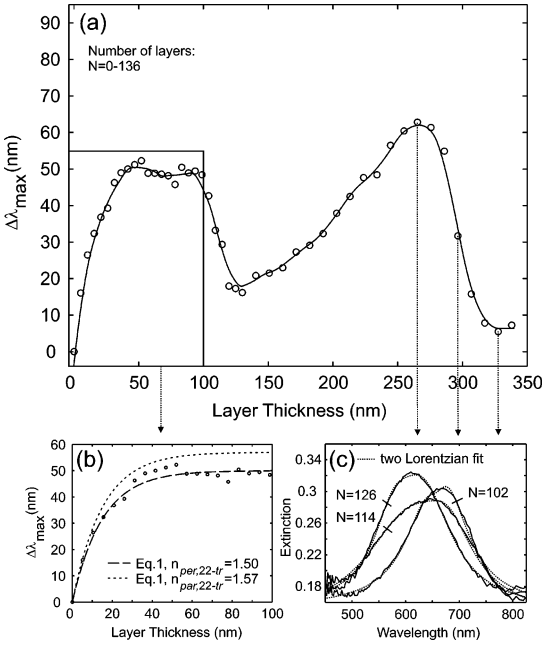

Figure 3. Summary of LSPR variation induced by an increasing layer thickness for gold nanodisks. (a) Relative LSPR shift plotted as a function of the dielectric layer thickness *d*. The solid line is a guide for the eye only. (b) Comparison between experiment and the exponential decay modes for the LSPR shift, using two refractive index values for the dielectric layer, in the region $d = 0-100$ nm. (c) Illustration of line-shape changes and broadening effects in the region of rapid blue-shifting.

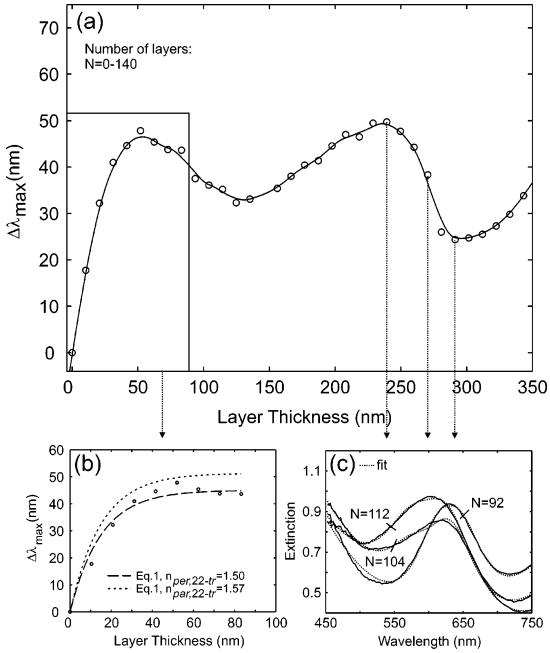

Figure 4. Same as in Figure 3 but for the short range ordered nanoholes in a 20 nm gold film.

increasing coating thickness. However, for $N \gtrsim 40$ and $d \gtrsim 100$ nm, where *d* is the total coating thickness, the LSPR spectra begin to blue-shift and then exhibit a periodic oscillation. This behavior is accompanied by a fluctuating peak shape. In particular, the line width of the LSPR becomes anomalously broad when the blue-shifting occurs. The same kinds of effects are seen for the short range ordered nanohole structures, see Figure 2b. Before analyzing the optical response for thick dielectric layers ($d > 100$ nm), it is important to focus on the well-studied region ($d < 100$ nm) and compare the results to previous experimental studies.[34] In Figure 3a, the LSPR shift in relation to the uncoated case, $\Delta\lambda_{max}(d)$, for the nanodisk samples, is shown. In many cases,[35−38] the short rage sensitivity to refractive index changes can be approximated by a model for surface plasmons on a planar metal surface. The LSPR wavelength shift is then expected to decrease exponentially as a function of coating thickness according to

$$\Delta\lambda_{max} = m\Delta n[1 - \exp(-d/L)] \quad (1)$$

Here *m* is the refractive index sensitivity $\delta\lambda_{max}/\delta n$, obtained from measurements in different uniform refractive index environments, Δn is the difference in refractive indices between the thin layer and the surrounding medium, *d* is the layer thickness, and *L* is the characteristic decay length of the local electromagnetic field surrounding the plasmonic nanostructure. Using eq 1, the Au nanodisk LSPR shift can be well reproduced using previously measured values for the different parameters, i.e., the thickness of the adsorbate layer being $d = N2.6$ nm,[39] $m = 100$ nm,[30] $\Delta n = 0.50$, or 0.57 and $L = 15$ nm;[34,40] see Figure 3b. The two values for Δn are motivated by the fact that 22-tricoscenoic acid is anisotropic, with $n = 1.57$ parallel and $n = 1.50$ perpendicular to the substrate, respectively. Both values give good agreement with the experimental data, as can be seen in Figure 3b. Equation 1 predicts that the LSPR shift should saturate at $\Delta\lambda_{max} = m\Delta n \approx 50-57$ nm for $d \gtrsim 50$ nm. However, this is clearly not the case. For $d > 100$ nm, the LSPR displays a dramatic oscillatory behavior, with a periodicity and amplitude of $d_p \approx 190$ nm and $\Delta\lambda_{amp,max} \approx 45$ nm, respectively. It is also clear that the oscillation is anharmonic; that is, the plasmon shift is much faster in the blue-shifting regions (at around $d \approx 120$ and 280 nm) than in the region between ∼150 and 250 nm, see Figure 3a. A closer look at the spectra in Figure 2 shows that these fast shifting regions are also characterized by broader and asymmetric line shapes. This is highlighted in Figure 3c, which compares spectra for $N = 102$, 114, and 126.

Figure 4a shows the variation in the nanohole extinction peak maximum obtained from the spectra displayed in Figure 2b. As in the case of the gold nanodisks, the $d < 100$ nm region can be well described using eq 1, see Figure 4b. A refractive index sensitivity $m = 90$ nm and a characteristic decay length $L = 15$ nm from ref 21 obviously yield good agreement with experimental data. For $d > 100$ nm, $\Delta\lambda_{max}$ again exhibits an oscillatory behavior with a period close to $d_p \approx 180$ nm, similar to the result for the gold nanodisks. Although the amplitude of the LSPR oscillations for the nanohole structure $\Delta\lambda_{amp,max} \approx 25$ nm is somewhat smaller than for disks, one notes a similar anharmonic variation in $\Delta\lambda_{max}(d)$. One also notes a similar broadening in the blue-shifting regions.

Figure 5a,b shows the numerical derivatives of $\Delta\lambda_{max}$ with respect to the layer thickness *d*. The most sensitive thickness regions, corresponding to the rapid blue-shift and marked with *s* in the graph, occur at $d \approx 100$ nm and $d \approx 290$ nm for the disks and at slightly lower thicknesses for the holes. We note that the sensitivities in these fast-shifting regions, of the order $\delta\Delta\lambda_{max}/\delta d \approx 1$ or above, are only a factor of 2−3 lower than what is found close to the metal surface.[21] This may have implications for novel LSPR sensor constructs, as mentioned below.

3.2. Interpretation. The LSPR $\Delta\lambda_{max}(d)$ curves for the two types of nanostructures clearly display very similar patterns. In the following, we will focus on the optical response of the gold nanodisks, for which the assignment of the optical resonance to a dipolar LSPR is well established.[1] This allows one to

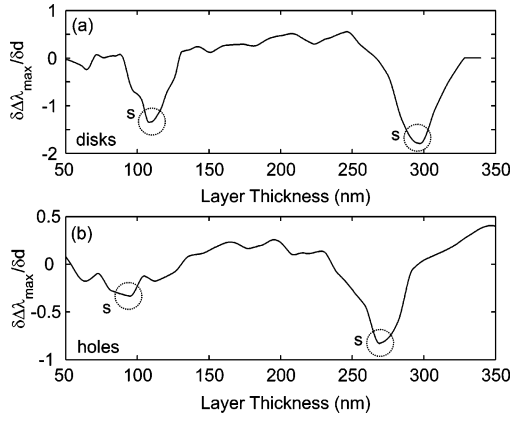

Figure 5. Derivative of the experimental $\Delta\lambda_{max}(d)$ values with respect to d for (a) nanodisks and (b) nanoholes. The part of the graph marked with the sign s indicates regions that are the most sensitive to a change in the dielectric layer thickness.

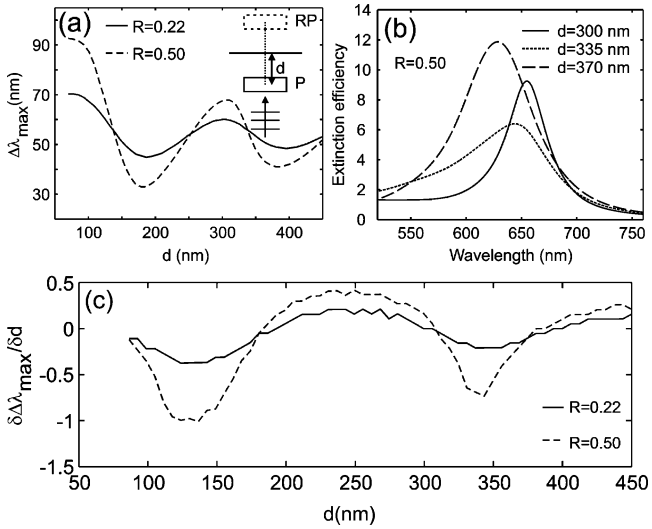

Figure 6. (a) Theoretical prediction of the extinction peak shift $\Delta\lambda_{max}$ as a function of dielectric layer thickness, d, from the image-dipole model, which is shown schematically in the inset. (b) Illustration of extinction spectra for $R = 0.50$ and d values within the blue-shifting region. (c) Theoretical derivatives of the $\Delta\lambda_{max}$ versus d curves is plotted versus layer thickness for $R = 0.22$ and 0.50.

formulate a simple physical picture of the observed phenomena using the image-dipole model, illustrated in the inset of Figure 6c. A similar approach was used by Holland et al.[24] to interpret LSPR frequency shifts observed for Ag and Au islands placed near a silver surface. We assume that the refractive indices of the LB film ($n = 1.50-1.57$) and the glass substrate ($n = 1.52$) are so close that we can neglect multiple reflections between the LB−air and the LB−glass interfaces. We then approximate the nanodisk as a point dipole oscillator that is affected by the field reflected back from the dielectric-air interface. The dipole moments for the particle P_P and its image P_I can then be defined as

$$P_P = \alpha(E_0(1 + R\cos(k2d)) + AP_I)$$

$$P_I = RP_P \qquad (2)$$

Here, α is the nanodisk polarizability, E_0 is the incident field, $AP_I = (1/(2d)^3 - ik/(2d)^2 - k^2/2d)\exp(ik2d)P_I$ is the image dipole field, which simulates the field reflected back to the nanodisk due to the 22-tricosenoic acid-air interface, $R = 0.22$ is the amplitude reflection coefficient at the dielectric−air interface, d is the distance to the interface, and $k = \omega/c_0 n$ is the wavevector of the optical field within the dielectric medium. The coupled dipole equation leads to an expression for the effective particle polarizability

$$\alpha_{eff} = \alpha\frac{1 + R\cos(k2d)}{1 - \alpha AR} \qquad (3)$$

A gold nanodisk is then approximated by an oblate spheroid and the polarizability is corrected for radiation damping.[30] This yields

$$\alpha = \frac{\tilde{\alpha}}{1 - \frac{ik^3\tilde{\alpha}}{6\pi}} \qquad (4)$$

where $\tilde{\alpha}$ is the quasi-static spheroid polarizability given by[1]

$$\tilde{\alpha} = 4\pi a^2 c\frac{\epsilon_s - \epsilon_m}{3\epsilon_m + 3L(\epsilon_s - \epsilon_m)} \qquad (5)$$

Here, a and c are the long and the short axis radii of the spheroid, ϵ_s is the complex dielectric function of gold, and $\epsilon_m = n^2$ is the dielectric constant of the surrounding medium. L is the spheroid shape factor, which can be calculated from the disk aspect ratio a/c.[1] In order to compare the theoretical model with the experimental extinction spectra, we calculate the effective extinction efficiency for various layer thicknesses d. This is given by the sum of the extinction efficiencies for the particle and its image, which yields

$$C_{ext} = k(1 + R)Im[\alpha_{eff}]/(\pi a^2) \qquad (6)$$

Figure 6 shows the LSPR shift vs d for an oblate Au spheroid that is 70 nm in diameter and 20 nm in height using the formalism described above. The dielectric function for gold was taken from Johnson and Christy,[41] and the refractive index of the dielectric environment was set to $n = 1.52$. The reference ($d = 0$) LSPR position, which defines $\Delta\lambda_{max} = 0$, is obtained from eq 4 using the average refractive index of glass and air, as the image-dipole model is not valid for very small d values. As is shown in Figure 6a (full line), the calculated $\Delta\lambda_{max}$ curve oscillates with a periodicity of ~200 nm, in good agreement with the experiment. However, the amplitude of the oscillation is significantly smaller than the measured one. As shown by the dashed curve in Figure 6a, a much better agreement is found if the reflection coefficient R is increased from $R = 0.22$ to 0.50. This change also results in an anharmonic oscillation, similar to that found in the experiments (i.e., with much more rapid changes in the blue-shifting regions than in the intermediate region). The change in R also gives a better agreement with the measured sensitivity to an increase in layer thickness d; compare Figures 5 and 6c.

The main argument behind artificially increasing R is that the diameter of the nanodisks or nanoholes are not much smaller than the thickness of the dielectric layers in reality. This means that the point dipole approximation, which is the basis behind eq 2, underestimates the field strength close to the particle surface. Further, the $1/2d$ far-field component of A, which dominates for large d values, can be expected to underestimate the directionality of the reflected field (a disk would rather act as a "nanomirror" for $d \approx 2a \lesssim \lambda$). These effects taken together lead to a too weak particle-image coupling, which is partly compensated for by artificially increasing R.

In order to further understand the spectral behavior, we keep only the radiative $1/2d$ term in A and assume that the particle polarizability α is approximately a Lorentzian $\alpha(\omega) = \alpha_0\omega_0/(\omega_0 - \omega - i\gamma)$, where α_0 is the DC polarizability, which is proportional to the particle volume, ω_0 is the eigenfrequency, and γ is a damping constant. By substituting this expression into eq 3, one finds that the resonance position is given by $\omega/\omega_0 = 1 + (\alpha_0 k^2 R)/2d \cos(k2d)$, which shows that the LSPR position oscillates as a function of d with a periodicity close to $\lambda_{max}/2n \approx 600/2 \times 1.5^2 = 200$ nm, where n is the refractive index of the dielectric layer. Similarly, the effective line-width is $\Gamma = \gamma - (\alpha_0 k^2 R\omega_0)/2d \sin(k2d)$, which exhibits maxima for $d \approx (2m - 1/2)\lambda_{max}/4n$, $m = 0, 1, 2...$ These distances correspond to the regions of maximum blue-shift, which explains the broadening found in Figures 3c and 4c.

4. Summary

We have studied the optical properties of short range ordered nanoholes and nanodisks as a function of overlayer thickness. By adsorbing 22-tricosenoic acid Langmuir−Blodgett films upon the nanostructures, we could follow the spectral variation up to a layer thickness of $d \approx 350$ nm. The LSPR peak position λ_{max} exhibits an oscillatory behavior with a period of $\sim\lambda_{max}/2n \approx 190$ nm, where n is the refractive index of the adsorbate. The spectral shifts versus coating thickness curves agree qualitatively with simulations based on a nanodisk polarizability renormalized through the image−dipole coupling model. However, the dipole model underestimates the coupling between the LSP and the interface, indicating the importance of finite size effects. The magnitude of the plasmon renormalization for large layer thicknesses, up to $\delta\Delta\lambda_{max}/\delta d \approx 2$ at $d \approx 290$ nm, suggests that these thick dielectric layers could be utilized in designing new types of bio/chemo sensors. By embedding the metal nanostructure in, for example, a layer of SiO_2 of optimal thickness ($d \approx 100$ or 290 nm), it should be possible to monitor molecular adsorption on the glass surface through the change in the LSPR spectrum. This construct would have at least three advantages in comparison to the classical, metal surface based, LSPR sensor. First, the sample would be easier to reuse, because it is easier to clean a glass surface than the metal (for example using a Piranha solution). Second, the glass layer would protect the metal nanostructures from various aging problems, including oxidation and solvent-induced nanoparticle reshaping effects.[34] Third, there would be no chemical contrast between different regions of the sensor surface, which would greatly facilitate the functionalization steps necessary for bio/chemo sensing experiments.

Acknowledgment. Funding of this work was provided by the Swedish Research Council and the Swedish Foundation for Strategic Research and supported by the European Union Network of Excellence PHOREMOST (Photons to Realize Molecular Scale Technologies). We thank Peter Johansson, Joan Alegret, Borja Sepulveda, and Javier Aizpurua for stimulating discussions and suggestions.

References and Notes

(1) Bohren, C. F.; Huffman, D. R. *Absorption and scattering of light by small particles*; John Wiley & Sons: New York, 1983.

(2) Kreibig, U.; Vollmer, M. *Optical Properties of Metal Clusters*; Springer: New York, 1995.

(3) Gunnarsson, L.; Rindzevicius, T.; Prikulis, J.; Kasemo, B.; Käll, M.; Zou, S.; Schatz, G. C. *J. Phys. Chem. B* **2005**, *109*, 1079−1087.

(4) Jensen, T. R.; Duyne, P. R. V.; Johnson, A. S.; Maroni, A. V. *Appl. Spectrosc.* **2000**, *54*, 371−377.

(5) Emory, R. S.; Nie, S. *J. Phys. Chem. B* **1998**, *102*, 493−497.

(6) Nie, S.; Emory, R. S. *Science* **1997**, *275*, 1102−1106.

(7) Yang, H. W.; Hulteen, C. J.; Schatz, C. G.; Duyne, P. R. V. *J. Phys. Chem.* **1996**, *104*, 4313−4323.

(8) Loo, C.; Lowery, A.; Halas, N.; West, J.; Drezek, R. *Nano Lett.* **2005**, *5*, 709−711.

(9) Elghanian, R.; Storhoff, J. J.; Mucic, C. R.; Letsinger, L. R.; Mirkin, A. C. *Science* **1997**, *277*, 1078−1081.

(10) Mock, J. J.; Smith, D. R.; Schultz, S. *Nano Lett.* **2003**, *3*, 485−491.

(11) Raschke, G.; Kowarik, S.; Franzl, T.; Sönnichsen, C.; Klar, T. A.; Feldmann, J.; Nichtl, A.; Kürzinger, K. *Nano Lett.* **2003**, *3*, 935−938.

(12) McFarland, A. D.; Duyne, R. P. V. *Nano Lett.* **2003**, *3*, 1057−1062.

(13) Haes, A. J.; Hall, W. P.; Chang, L.; Klein, W. L.; Duyne, R. P. V. *Nano Lett.* **2004**, *4*, 1029−1034.

(14) Haes, A. J.; Zou, S.; Schatz, G. C.; Duyne, R. P. V. *J. Phys. Chem. B* **2004**, *108*, 6961−6968.

(15) Mirkin, A. C.; Letsinger, L. R.; Mucic, C. R.; Storhoff, J. J. *Nature* **1996**, *382*, 607.

(16) Cao, W. Y.; Jin, C. R.; Mirkin, A. C. *Science* **2002**, *297*, 1536.

(17) Connolly, S.; Cobbe, S.; Fitzmaurice, D. *J. Phys. Chem. B* **2001**, *105*, 2222.

(18) Storhoff, J. J.; Lazarides, A. A.; Mucic, C. R.; Mirkin, A. C.; Letsinger, L. R.; Schatz, C. G. *J. Am. Chem. Soc.* **2000**, *122*, 4640.

(19) Miller, M. M.; Lazarides, A. A. *J. Phys. Chem. B* **2005**, *109*, 21556−21565.

(20) Xu, H.; Käll, M. *Sens. Actuators B* **2002**, *87*, 244−249.

(21) Rindzevicius, T.; Alaverdyan, Y.; Dahlin, A.; Höök, F.; Sutherland, D.; Käll, M. *Nano Lett.* **2005**, *5*, 2335−2339.

(22) Haynes, C. L.; et al. *J. Phys. Chem. B* **2003**, *107*, 7337−7342.

(23) Zou, S.; Janel, N.; Schatz, G. C. *J. Chem. Phys.* **2004**, *120*, 10871−10875.

(24) Holland, W. R.; Hall, D. G. *Phys. Rev. Lett.* **1984**, *52*, 1041−1044.

(25) Murray, W. A.; Suckling, J. R.; Barnes, W. L. *Nano Lett.* **2006**, *6*, 1772−1777.

(26) Chance, R. R.; Prock, A.; Silbey, R. *Phys. Rev. A* **1975**, *12*, 1448−1452.

(27) Hanarp, P.; Sutherland, D. S.; Gold, J.; Kasemo, B. *Colloids Surf. A* **2003**, *214*, 23−36.

(28) Prikulis, J.; Hanarp, P.; Olofsson, L.; Sutherland, D.; Käll, M. *Nano Lett.* **2004**, *4*, 1003−1007.

(29) Dahlin, A.; Zäch, M.; Rindzevicius, T.; Käll, M.; Sutherland, D.; Höök, F. *J. Am. Chem. Soc.* **2005**, *127*, 5043−5048.

(30) Hanarp, P.; Käll, M.; Sutherland, D. S. *J. Phys. Chem. B* **2003**, *107*, 5768−5772.

(31) Rindzevicius, T.; Alaverdyan, Y.; Sepulveda, B.; Pakizeh, T.; Käll, M.; Hillenbrand, R.; Aizpurua, J.; de Abajo, F. J. G. *J. Phys. Chem. C* **2007**, *111*, 1207−1212.

(32) Amos, R. M.; Barnes, W. L. *Phys. Rev. B* **1997**, *55*, 7249−7254.

(33) Garrett, S.; Wasey, J. A. E.; Barnes, W. L. *J. Mod. Opt.* **2005**, *52*, 1105−1122.

(34) Malinsky, M. D.; Kelly, K. L.; Schatz, G. C.; Duyne, R. P. V. *J. Am. Chem. Soc.* **2001**, *123*, 1471−1482.

(35) Haes, A. J.; Duyne, R. P. V. *J. Phys. Chem. Soc.* **2002**, *124*, 10596−10604.

(36) Haes, A. J.; Chang, L.; Klein, W. L.; Duyne, R. P. V. *J. Phys. Chem. Soc.* **2005**, *127*, 2254−2271.

(37) Riboh, J. C.; Haes, A. J.; McFarland, A. D.; Yonzon, C. R.; Duyne, R. P. V. *J. Phys. Chem. B* **2003**, *107*, 1772−1780.

(38) Jeoung, C. R. Y. E.; Zou, S.; Schatz, G. C.; Mrksich, M.; Duyne, R. P. V. *J. Phys. Chem. Soc.* **2004**, *126*, 12669−12676.

(39) Barnes, W. L.; Sambles, J. R. *Surf. Sci.* **1986**, *177*, 399−416.

(40) Hillenbrand, R.; Keilmann, F.; Hanarp, P.; Sutherland, D. S.; Aizpurua, J. *Appl. Phys. Lett.* **2003**, *83*, 368−370.

(41) Johnson, P. B.; Christy, R. W. *Phys. Rev. B* **1972**, *6*, 4370−4379.